

Quantum and classical approaches to the optimization of highway platooning: the two-vehicle matching problem

Chinonso Onah^{1,2}[0000-0002-6296-533X],
 Agneev Guin^{1,4}[0000-0001-7065-2192],
 Carsten Othmer¹[0009-0009-3534-371X],
 J. A. Montañez-Barrera³[0000-0002-8103-4581], and
 Kristel Michielsen^{2,3}[0000-0003-1444-4262]

¹ Volkswagen AG, Berliner Ring 2, Wolfsburg 38440, Germany
 {chinonso.calistus.onah, agneev.guin, carsten.othmer}@volkswagen.de

² Department of Physics, RWTH Aachen University, Germany

³ Jülich Supercomputing Centre, Forschungszentrum Jülich, Germany
 {j.montanez-barrera,k.michielsen}@fz-juelich.de

⁴ Department of Network Engineering, BarcelonaTech (UPC), Spain

Abstract. Aerodynamic drag reduction on highways through vehicle platooning is a well-known concept that has not seen systematic uptake so far. Arguably because of high technological and legislative obstacles. As a low-tech entry solution to real multi-vehicle platooning, “Windbreaking-as-a-Service” (WaaS) was introduced in [20]. Here we leverage the QUBO formulation to explore classical meta-heuristics such as simulated annealing, tabu search, and emergent quantum heuristics including quantum annealing and variants of the Quantum Approximate Optimization Algorithm (QAOA). These heuristic solvers do not guarantee optimality, yet they traverse the same high-order landscape in polynomial memory. They can be parallelized aggressively, and efficient classical processing can be employed to return *only* valid schedules in certain hybrid workflows. The present paper therefore positions QUBO as the *lingua franca* that allows heterogeneous classical, quantum and hybrid solvers to attack the optimization of highway platooning.

Keywords: quantum optimization; QUBO; aerodynamics; platooning; CO₂ mitigation

1 Problem Formulation

1.1 Matching Problem Statement

We study the two-vehicle matching problem on a single road segment formulated in [20]. A *surfer* is a vehicle that seeks to follow (or be assigned to) a compat-

ible lead vehicle, a *breaker* for cooperative driving. The *breaker* can accept at most one *surfer* for such an assignment. The overall objective is to compute a one-to-one (or capacity-respecting) matching between surfers and breakers that minimizes a weighted cost capturing aerodynamic efficiency and timing/velocity compatibility. The a mathematical statement is the following:

Let the set of surfers be $\mathcal{S} = \{1, \dots, S\}$ and the set of breakers be $\mathcal{B} = \{1, \dots, B\}$. We form a bipartite graph $G(\mathcal{S} \cup \mathcal{B}, \mathcal{E})$ where each edge $(s, b) \in \mathcal{E}$ indicates that surfer $s \in \mathcal{S}$ can potentially be matched to breaker $b \in \mathcal{B}$. For each possible edge $(s, b) \in \mathcal{E}$, we define a binary variable $x_{s,b} \in \{0, 1\}$ such that:

$$x_{s,b} = \begin{cases} 1, & \text{if surfer } s \text{ is assigned to breaker } b, \\ 0 & \text{otherwise.} \end{cases}$$

The edge carries a weight $w_{s,b}$ reflecting the aerodynamic efficiency and timing compatibility of the pairing. It is defined as:

$$w_{s,b} = c_s V_b^2 [1 - f(C_b - c_s)] + \lambda_1 \Delta_{s,b}^T + \lambda_2 \Delta_{s,b}^V, \quad (1)$$

where $\lambda_1, \lambda_2 \geq 0$ are scaling factors, and $\Delta_{s,b}^T$ and $\Delta_{s,b}^V$ capture time and velocity preferences of surfer s for breaker b as follows:

$$\Delta_{s,b}^T = \begin{cases} |t_s - T_b| & \text{if } |t_s - T_b| > \delta t_s / 2, \\ 0 & \text{otherwise,} \end{cases} \quad (2)$$

and similarly for $\Delta_{s,b}^V$, with δt_s and δv_s being surfer-individual flexibility intervals for departure time and preferred travel speed, respectively.

The matching problem is therefore formalized in [20] as:

$$\min_{x_{s,b} \in \{0,1\}} \sum_{s \in \mathcal{S}} \sum_{b \in \mathcal{B}} w_{s,b} x_{s,b} \quad (3)$$

subject to constraints:

$$\begin{aligned} \sum_{b \in \mathcal{B}} x_{s,b} &= 1, \quad \forall s \in \mathcal{S} \quad (\text{each surfer matched exactly once}) \\ \sum_{s \in \mathcal{S}} x_{s,b} &= 1, \quad \forall b \in \mathcal{B} \quad (\text{each breaker matched at most once}) \end{aligned} \quad (4)$$

i.e. we require each surfer $s \in \mathcal{S}$ to be matched to exactly one breaker, and each breaker $b \in \mathcal{B}$ to accept exactly one surfer. We further assume $B = S$ in the rest of the paper.

1.2 QUBO Form

To exploit quantum and quantum-inspired solvers, we need to transform the problem into a QUBO problem. To that end, we add squared-penalty terms

with a hyperparameter λ_3 to quadratize the constraints and obtain the following unconstrained version:

$$\lambda_3 \sum_{s \in \mathcal{S}} \left(1 - \sum_{b \in \mathcal{B}} x_{s,b}\right)^2 + \lambda_3 \sum_{b \in \mathcal{B}} \left(1 - \sum_{s \in \mathcal{S}} x_{s,b}\right)^2. \quad (5)$$

This is added to Eq. (3) to yield the QUBO problem. Namely:

$$\min_{\{x_{s,b}\}} \left(\sum_{(s,b) \in \mathcal{E}} w_{s,b} x_{s,b} + \lambda_3 \sum_{s \in \mathcal{S}} \left(1 - \sum_{b \in \mathcal{B}} x_{s,b}\right)^2 + \lambda_3 \sum_{b \in \mathcal{B}} \left(1 - \sum_{s \in \mathcal{S}} x_{s,b}\right)^2 \right).$$

With $n := S(= B)$, we can list all pairs (s, b) in a vector:

$$x = (x_{1,1}, x_{1,2}, \dots, x_{1,n}, x_{2,1}, \dots, x_{n,n})^T.$$

Eq. (6) becomes the standard form as mentioned in [20]:

$$\min x^T Q x \quad (6)$$

$$\text{with } Q_{ee} = w_{s,b} + \lambda_1 \Delta_{s,b}^T + \lambda_2 \Delta_{s,b}^V - 2\lambda_3$$

$$\text{and } Q_{ee'} = \begin{cases} \lambda_3 & \text{if } e \text{ and } e' \text{ share a node} \\ 0 & \text{otherwise.} \end{cases}$$

This QUBO matrix has an interesting tensor structure. To see that, let $Q \in \mathbb{R}^{n^2 \times n^2}$ and

$$Q = \text{diag}_{n^2}(w_{s,b} - 4\lambda_3) + \lambda_3 (I_N \otimes J_N + J_N \otimes I_N) \quad (7)$$

where $I_N : N \times N$ identity matrix

$$\text{and } J_N : N \times N \text{ "1"-matrix} = \begin{pmatrix} 1 & 1 & \dots & 1 \\ 1 & 1 & \dots & 1 \\ \vdots & \vdots & \ddots & \vdots \\ 1 & 1 & \dots & 1 \end{pmatrix}$$

This structure is closely related to the fact that valid solutions can be translated into permutation matrices. This is a property that can be leveraged to improve the quantum solution both in speed and accuracy. (Refer Sec. 2.7 and [18]).

Constraints and Energy Landscape Analysis We seek a small enough penalty weight λ_3 that guarantees all invalid one-hot assignments lie strictly above all valid ones in the QUBO energy landscape. To derive this, let the

matrix representation of the problem $C = [c_{ij}] \in \mathbb{R}^{n \times n}$. The maximum possible cost-saving from swapping any one assignment is

$$c_{\max} - c_{\min},$$

and there are n rows (or columns) whose one-hot constraints could be violated. Hence any invalid bitstring can gain at most $n(c_{\max} - c_{\min})$ in the cost term. By choosing

$$\lambda_3 > n(c_{\max} - c_{\min}),$$

we ensure that the penalty for violating even one one-hot constraint outweighs *all* possible cost savings from invalid assignments. Multiplying by a *safety* factor > 1 yields a strict separation without unduly inflating the penalty.

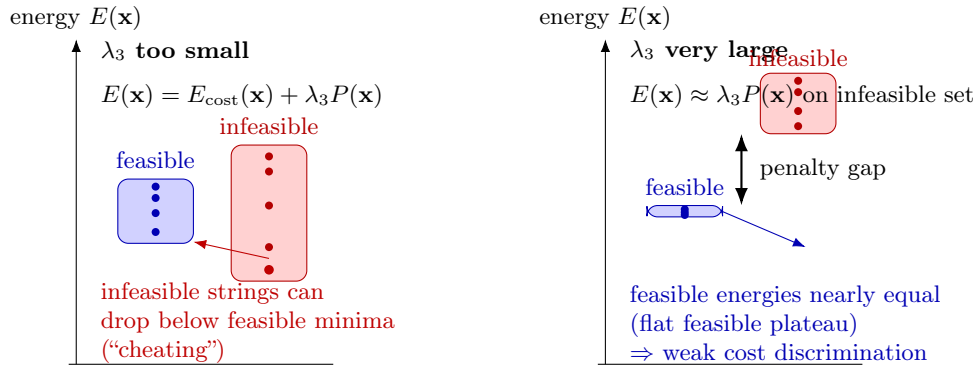


Fig. 1: Schematic energy landscape under two penalty-weight regimes. Left: if λ_3 is too small, infeasible configurations can “cheat” by lowering E_{cost} enough to overcome penalties. Right: if λ_3 is very large, infeasible states are pushed far above the feasible manifold, but feasible energies compress into an almost flat plateau, reducing cost discrimination among valid matchings.

As shown in Fig. 1, when λ_3 is too small compared to the spread of $c_{i,j}$, then the sampler can *reduce* E_{cost} by picking invalid assignments (e.g. two ones in the same row), because the small penalty is outweighed by cost savings. This produces noisy, infeasible solutions that cheat the one-hot rule in Eq. (4).

Mapping the QUBO to a Quantum Hamiltonian To solve an optimization problem on a quantum computer, its QUBO formulation must be mapped to a quantum Hamiltonian [12]. This is derived in the standard way by expressing a symmetric QUBO matrix in terms of its components and transforming the upper triangular part into an Ising Hamiltonian. In this formalism, each qubit in the computational basis corresponds to a binary variable and hence an edge (s, b) in the bipartite graph picture. Consider the following generic QUBO matrix:

$$x^T Q x = \sum_{i,j} Q_{ij} x_i x_j \quad (8)$$

where $x_i \in \{0, 1\}$ are binary variables, and Q_{ij} is the matrix defining the quadratic coefficients. Each binary variable x_i is mapped to a qubit using the relation:

$$x_i = \frac{1}{2}(I - Z_i) \quad (9)$$

where Z_i is the Pauli-Z operator acting on the i -th qubit, and I is the identity operator, effectively transforming the binary variable x_i into a Pauli-Z operator. See Ref [12] for details. The full Hamiltonian becomes

$$H = \sum_i \frac{Q_{ii}}{2}(I - Z_i) + \sum_{i < j} \frac{Q_{ij}}{4}(I - Z_i - Z_j + Z_i Z_j). \quad (10)$$

The constant identity terms do not influence the optimization landscape of the QUBO problem and can be omitted.

1.3 Performance metrics

Because heuristic samplers return *distributions* rather than proofs of optimality, a single scalar such as the “best cost” gives an incomplete—and occasionally misleading—picture of performance. A solver call returns N raw samples (“reads”) of bitstrings $\mathbf{x}_k \in \{0, 1\}^{N_{\text{vars}}}$ ⁵, their QUBO energies $E_k \equiv E(\mathbf{x}_k)$, and quadratic penalties $P(\mathbf{x}_k)$ which vanish only for feasible matchings (Refer Sec. 1). We denote by E_* the exact ground-state energy obtained from the Hungarian algorithm and the corresponding MIQP (mixed-integer quadratic program) baseline (Refer Sec. 2.2). Following the benchmarking practice of Refs. [23,24], we log an additional battery of complementary metrics for different solvers and aggregate them for further statistical analyses. The following metrics are considered.

1. Best energy:

$$E_{\text{best}} = \min_k E_k.$$

This is the smallest energy observed in a batch and is the headline quality indicator: if $E_{\text{best}} = E_*$, the sampler has, at least once, hit a global optimum (up to degeneracy). Because this metric is sensitive to rare outliers, we always report it alongside aggregate statistics.

2. Mean energy:

$$\langle E \rangle = \frac{1}{N} \sum_{k=1}^N E_k.$$

The mean energy smooths out incidental hits and captures the typical quality an end user would obtain by accepting the first sample supplied by the solver.

⁵ N_{vars} is the number of binary variables in the problem and thus the length of the bitstring

3. **Optimality gaps:** When an exact optimum E_* is available (via the Hungarian or MIQP baselines), we quantify absolute solution quality through relative gaps

$$\Delta_{\text{best}} = \frac{E_{\text{best}} - E_*}{|E_*|}, \quad \Delta_{\text{mean}} = \frac{\langle E \rangle - E_*}{|E_*|}.$$

4. **Energy variance:**

$$\sigma_E^2 = \frac{1}{N} \sum_{k=1}^N (E_k - \langle E \rangle)^2.$$

High σ_E^2 indicates broad exploration of the energy landscape; low variance indicates a sharply peaked output distribution, which may reflect successful concentration around good minima—or, conversely, premature convergence to a poor local basin. We therefore interpret this metric in conjunction with the gaps and success probability.

5. **Single-shot success probability (ground-state probability):** The success probability is defined as

$$p_{\text{succ}} := \Pr_{\mathbf{x} \sim \pi} [E(\mathbf{x}) = E_* \wedge P(\mathbf{x}) = 0], \quad (11)$$

Empirically, we estimate it from a batch of N samples $\{\mathbf{x}_k\}_{k=1}^N$ as

$$\hat{p}_{\text{succ}} = \frac{\#\{k : E(\mathbf{x}_k) = E_* \wedge P(\mathbf{x}_k) = 0\}}{N},$$

i.e. the fraction of all samples that are feasible and achieve the ground-state energy. If the ground state of the problem Hamiltonian is degenerate, two or more bitstrings that correspond to different matching outcomes can attain this energy value. This scenario is further discussed in Sec. 3 where one readily observes different assignments that match the same MIQP energy leading to different energy-saving outcomes compared to the MIQP and Hungarian outcomes.

6. **Samples-to-solution (STS)** For independent samples, the expected number of draws needed to observe a single optimum is the mean of a geometric distribution,

$$\text{STS} := \frac{1}{p_{\text{succ}}}, \quad (12)$$

as in Eq. (12). In practice we plug in the empirical estimate \hat{p}_{succ} . STS is backend-agnostic: it depends only on the sampler’s quality, not on device speed.

1.4 Benchmark Dataset

We publish a small companion dataset containing ten single-segment matching instances with $n \in \{3, \dots, 12\}$ surfer-breaker pairs. For each n we provide two

NumPy arrays, `n-vehicles-breakers.npy` and `n-vehicles-surfers.npy`. The breaker array stores, per vehicle, its class label, cruising velocity, and departure time, while the surfer array stores the surfer’s class, preferred velocity, departure time, and individual flexibility intervals for speed and departure time. These instances are used to construct the edge weights $w_{s,b}$ and the corresponding QUBO matrices Q for all experiments reported in this work. A python script for manipulating the data is also provided. The dataset is versioned and publicly available at <https://doi.org/10.5281/zenodo.17768136>[19]. The dataset is used for the tables and figures in Sec. 2 and 3.

2 Quantum-(Inspired) Optimization Methods

All seven solvers in our “solver zoo” act on the same combinatorial object: either the linear assignment problem of Eqs. (3)–(4) or its QUBO reformulation in Eqs. (6)–(7). For the latter, it is convenient to write

$$E(\mathbf{x}) = \mathbf{x}^T Q \mathbf{x}, \quad \mathbf{x} \in \{0, 1\}^N, \quad N = n^2, \quad (13)$$

with ground-state energy $E_\star = \min_{\mathbf{x}} E(\mathbf{x})$. Each heuristic solver defines (implicitly) a probability distribution $\pi(\mathbf{x})$ over bitstrings.

2.1 Hungarian assignment algorithm: exact polynomial baseline

The Hungarian algorithm solves the linear assignment problem

$$\begin{aligned} \min_{x_{ij}} \quad & \sum_{i=1}^n \sum_{j=1}^n c_{ij} x_{ij}, & (14) \\ \text{s.t.} \quad & \sum_{j=1}^n x_{ij} = 1, \quad i = 1, \dots, n, \\ & \sum_{i=1}^n x_{ij} = 1, \quad j = 1, \dots, n, \\ & x_{ij} \in \{0, 1\}, \end{aligned}$$

in strongly polynomial time $\mathcal{O}(n^3)$ [11]. In our setting, c_{ij} corresponds to the edge weights $w_{s,b}$ on a single road segment, i.e. the cost term of Eq. (3) without quadratic penalties. Because all feasible matchings satisfy the one-hot constraints, the minimizer of Eq. (14) coincides with the ground state of the QUBO energy restricted to the feasible subspace.

We therefore treat the Hungarian method as our *exact polynomial baseline*: it delivers the provably optimal two-vehicle matching on each road segment, and its optimal value E_{Hung} serves as the reference against which we measure optimality gaps of all heuristic solvers,

$$\Delta_{\text{best}} = \frac{E_{\text{solver}} - E_{\text{Hung}}}{|E_{\text{Hung}}|} \times 100\%. \quad (15)$$

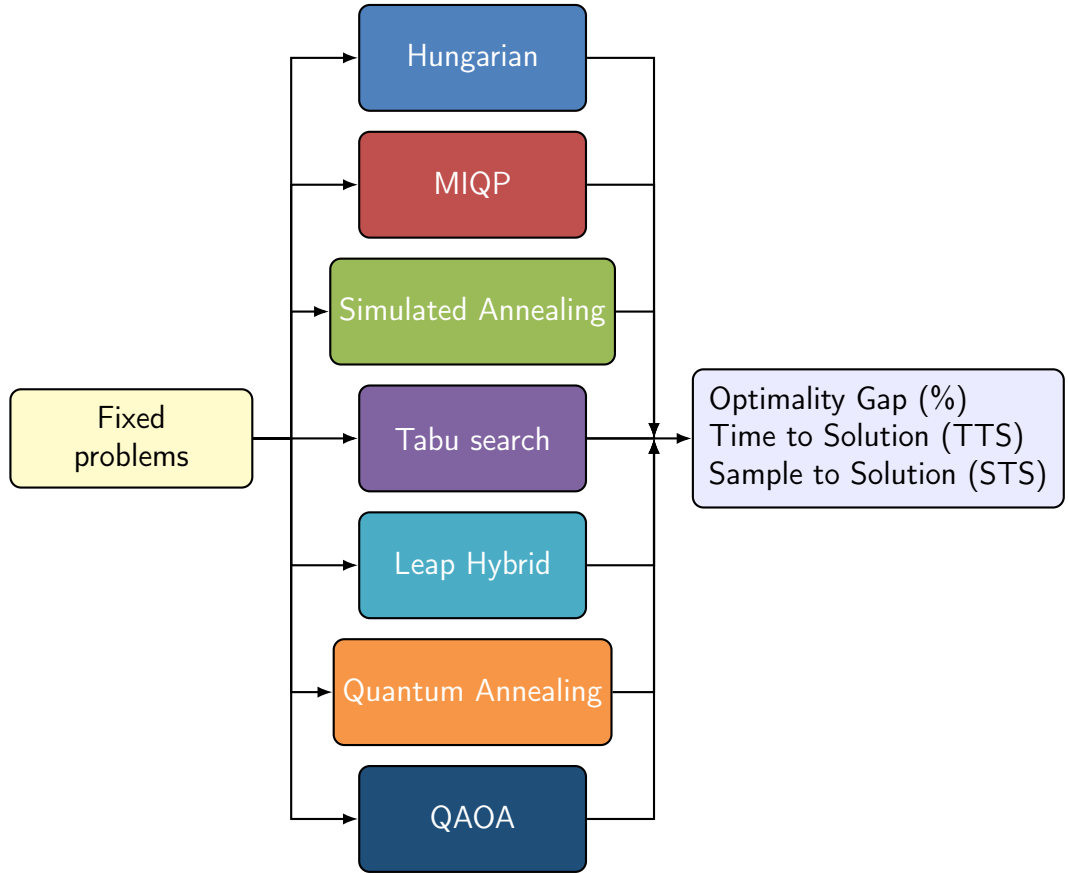


Fig. 2: “Solver-zoo” benchmark. Every solver is run on the **same fixed problem sets** (yellow), and all outputs are funneled into one **common metric panel** (purple) for direct comparison.

Hungarian baseline in the metrics language: The Hungarian algorithm is an *exact* polynomial-time solver for the linear assignment problem. On each instance it returns a unique optimal matching \mathbf{x}_{Hung} that minimizes the linear cost in Eq. (14). When we embed this matching into the QUBO representation of Eq. (13) via the row-major bitstring $\mathbf{x}_{\text{Hung}} \in \{0, 1\}^{n^2}$, its QUBO energy $E_{\text{Hung}} = E(\mathbf{x}_{\text{Hung}})$ coincides with the ground-state energy E_* restricted to the feasible subspace.⁶ As per the performance metrics of Sec. 1.3, this implies

$$p_{\text{succ}} = 1, \quad \text{STS} = \frac{1}{p_{\text{succ}}} = 1.$$

⁶ Modulo the rescaling factors used to normalize the Ising Hamiltonian in Sec. 2.5.

Every call to the Hungarian solver returns a feasible ground state, so the best and mean energies coincide,

$$E_{\text{best}} = \langle E \rangle = E_{\text{Hung}}, \quad \sigma_E^2 = 0,$$

and the optimality gaps Δ_{best} and Δ_{mean} also vanish by construction.

2.2 Gurobi MIQP solver

To obtain an exact baseline at the QUBO level, we also formulate the problem as a mixed-integer quadratic program (MIQP). Introducing a binary decision vector $\mathbf{z} \in \{0, 1\}^N$ that coincides with \mathbf{x} , the MIQP reads

$$\begin{aligned} \min_{\mathbf{z}} \quad & \frac{1}{2} \mathbf{z}^\top H \mathbf{z} + \mathbf{f}^\top \mathbf{z}, \\ \text{s.t.} \quad & A\mathbf{z} = \mathbf{b}, \\ & \mathbf{z} \in \{0, 1\}^N, \end{aligned} \tag{16}$$

where H and \mathbf{f} are constructed from the QUBO matrix Q (up to a constant shift) and $A\mathbf{z} = \mathbf{b}$ encode the one-hot constraints explicitly instead of via penalties. In practice we use the Gurobi Optimizer in MIQP mode [22], which combines presolve reductions, cutting planes, heuristics, and branch-and-bound/branch-and-cut tree search to obtain provably optimal solutions or certified bounds on $E_{\mathbf{x}}$.

For the problem sizes considered here, MIQP remains tractable and yields the optimal energy E_{MIQP} , a certified lower bound E_{LB} and the corresponding *MIQP gap*. We verify the optimality by matching the corresponding assignment cost with E_{Hung} . The *MIQP gap* is the relative optimality gap reported by Gurobi [22], and is defined by

$$\text{MIQP gap} = \frac{|E_{\text{best}} - E_{\text{LB}}|}{|E_{\text{best}}|}$$

MIQP thus provides a second, independent correctness oracle for the heuristic solvers and is consistent with recent work on quantum-ready routing formulations [7]. The MIQP provided the necessary baseline for benchmarking results reported in Figs. 3 and 8.

2.3 Simulated annealing (SA): thermodynamic meta-heuristic

Simulated annealing (SA) is a stochastic local-search heuristic inspired by thermodynamic cooling [10,4]. On a given QUBO energy $E(\mathbf{x})$ we define a single-spin-flip Markov chain over $\{0, 1\}^N$ at temperature $T > 0$. Starting from an initial configuration $\mathbf{x}^{(0)}$, one iteration proposes a neighbor \mathbf{x}' (e.g. by flipping a randomly chosen bit) and accepts it with Metropolis probability

$$p_{\text{acc}}(\mathbf{x} \rightarrow \mathbf{x}'; T) = \min\left\{1, \exp[-\Delta E/T]\right\}, \quad \Delta E = E(\mathbf{x}') - E(\mathbf{x}). \tag{17}$$

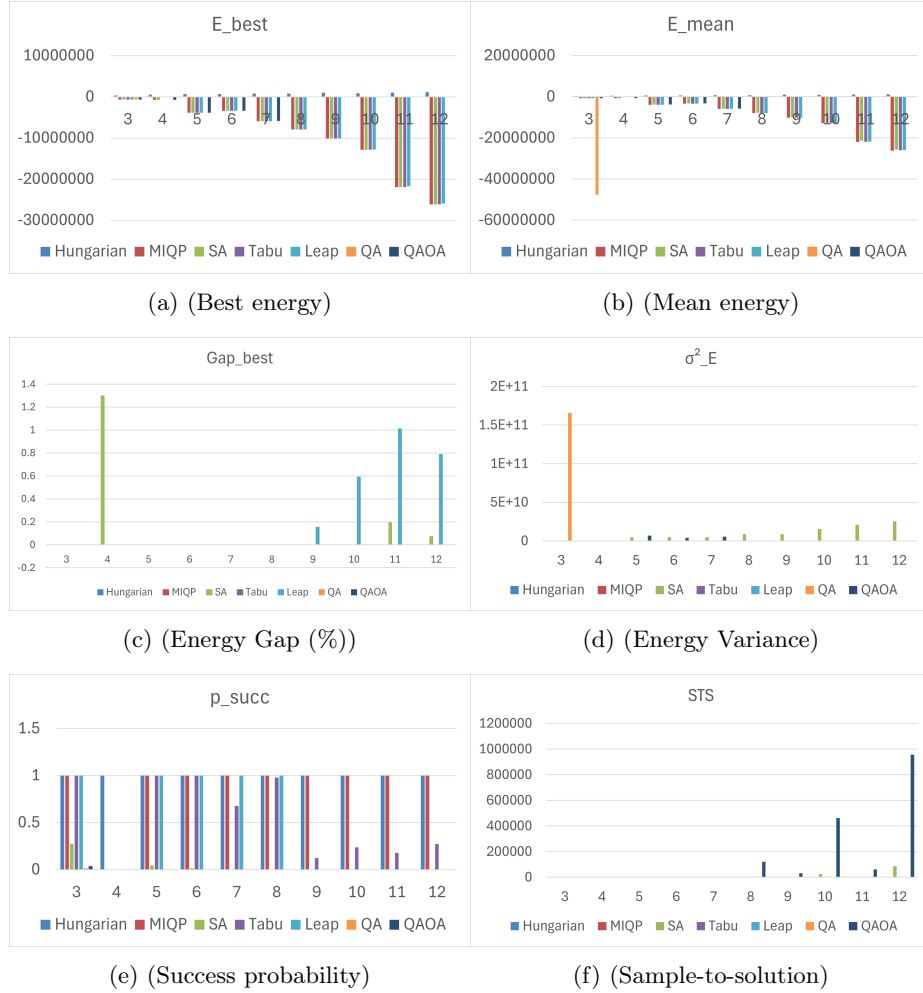


Fig. 3: Summary of solver performance metrics for 10 problem instances in the benchmark suite in Sec. 1.4. For a more detailed view of the benchmark results underlying these plots and Figs. 8, we refer the reader to the Supplementary Material App. A. It provides the full benchmarking tables for all instance sizes, including the raw and derived quantities used in the plots. These supplementary tables provide a reproducible reference for comparing the classical, quantum, and hybrid solvers.

At fixed temperature T , the chain has the Boltzmann distribution $\pi_T(\mathbf{x}) \propto e^{-E(\mathbf{x})/T}$ as stationary measure under mild connectivity conditions [4]. A *cooling schedule* T_0, T_1, \dots slowly decreases temperature and biases the sampling progressively towards low-energy configurations. In the limit of infinitely slow cooling (e.g. logarithmic schedules), SA converges to the global optimum in probability, but practical implementations use finite schedules with limited sweeps over the bitstring [10]. For our benchmark we implement SA directly on the QUBO, using single-bit neighborhoods, geometric cooling schedules, and multiple random restarts. SA related metrics are collected in Figs. 3 and 8.

2.4 Memory-based deterministic Tabu search

Tabu search is a deterministic local-search meta-heuristic that augments greedy descent with adaptive memory in order to escape local minima [5]. On the QUBO energy $E(\mathbf{x})$ we define a neighborhood $N(\mathbf{x})$ (here, Hamming-1 neighbors). Starting from $\mathbf{x}^{(0)}$ we iterate on the following steps:

1. generate all candidate moves $m \in N(\mathbf{x}^{(k)})$ and their energy changes $\Delta E(m)$;
2. discard moves that are *tabu*, i.e. whose inverse move is stored in a short-term tabu list \mathcal{T} of bounded length L ;
3. among the remaining moves, select the one with lowest resulting energy, even if $\Delta E > 0$;
4. update \mathcal{T} by inserting the chosen move (or its inverse) and possibly removing the oldest entry.

An *aspiration criterion* allows tabu moves that yield a new global best energy to override tabu status. The tabu list prevents short cycles and encourages exploration of new regions of the energy landscape, while the greedy choice enforces intensification around promising basins [5]. Within our benchmark we run tabu search directly on the QUBO with fixed tabu tenure L and a cap on the number of iterations per run. Both Tabu and SA are implemented with D-Wave SDK[13].

2.5 Quantum annealing (QA)

Quantum annealing (QA) is the quantum analogue of SA, implemented as a continuous-time evolution under a time-dependent Hamiltonian [9,13,2]. We first map the QUBO to an Ising model in Pauli- Z variables. Introducing spin variables $z_i \in \{-1, +1\}$ related to the bits by $x_i = \frac{1}{2}(1 - z_i)$. As worked out in Eq. (10), the QUBO energy can be rewritten (up to an additive constant) as

$$E(\mathbf{x}) = \text{const} + \sum_i h_i z_i + \sum_{i < j} J_{ij} z_i z_j, \quad (18)$$

which defines the problem Hamiltonian

$$H_P = \sum_i h_i \sigma_i^z + \sum_{i < j} J_{ij} \sigma_i^z \sigma_j^z. \quad (19)$$

Here σ_i^z is the Pauli- Z operator on qubit i . QA adds a transverse-field driver

$$H_D = - \sum_i \sigma_i^x, \quad (20)$$

and interpolates between them over annealing time T_{anneal} via

$$H(s) = A(s) H_D + B(s) H_P, \quad s = t/T_{\text{anneal}} \in [0, 1], \quad (21)$$

with $A(0) \gg B(0)$ and $A(1) \ll B(1)$. If the evolution is sufficiently slow and the minimum spectral gap is not exponentially small, the adiabatic theorem predicts that the system ends close to the ground state of H_P [2].

On D-Wave-like hardware, QA is realized as an open-system analogue of this process with fixed chip topology and limited coupling precision [13]. Our QUBOs are embedded onto the hardware graph and we sample bitstrings from the final measurement distribution, following the benchmarking philosophy of Refs. [23,24]. Repeated shots yield an empirical p_{succ} and thus STS via Eq. (12).

Remark on quantum annealing runs. For $n = 4$, QA (Refer Sec. 2.8 for tabu) did not produce any feasible solution within the allotted shot budget. Similarly, for $n \geq 5$, we observed no feasible solutions from QA samples; this likely reflects the combined effect of (i) embedding-related chain breaks (which become more prevalent as problem size increases) and (ii) the limited number of shots available under the account used for these runs. We therefore postpone a more extensive QA evaluation to future work.

2.6 Leap Hybrid Solver

The Leap Hybrid solver is a quantum-classical hybrid workflow provided via D-Wave’s Leap service [8]. It accepts QUBO (or more general quadratic models) at the user interface and internally orchestrates a decomposition across classical and quantum resources [13,24]. Conceptually, a large QUBO problem is partitioned into overlapping subproblems that fit onto the Quantum processing unit (QPU). The procedure involves three core steps:

1. **Decomposition:** partition the variable set into overlapping blocks and define sub-QUBOs;
2. **Subproblem optimization:** repeatedly send sub-QUBOs to the QPU (quantum annealing) and/or classical heuristics to propose improved assignments;
3. **Reconstruction:** reconcile subproblem solutions into a global assignment \mathbf{x} using classical coordination logic.

The hybrid engine automatically manages the trade-off between quantum calls and classical refinement subject to a user-specified wall-clock limit and returns a candidate bitstring and energy [8]. Similarly, we also record E_{hyb} , p_{succ} , STS and TTS in in Figs. 3 and 8.

2.7 QAOA: gate-model quantum optimization

Similar to quantum annealing, the Quantum Approximate Optimization Algorithm (QAOA) is a gate-model, hybrid quantum-classical algorithm that alternates between unitaries generated by the problem Hamiltonian (Eq. (10)) and a transverse-field mixing Hamiltonian (Eq. (20)). It was first proposed in [3]. Using the QUBO-derived problem Hamiltonian, conventionally denoted as H_C , and the driver Hamiltonian (conventionally denoted as H_M), the algorithm prepares the initial state $|\psi_0\rangle = |+\rangle^{\otimes N}$ and defines the unitary operators:

$$U_C(\gamma_\ell) = \exp(-i\gamma_\ell H_C), \quad (22)$$

$$U_M(\beta_\ell) = \exp(-i\beta_\ell H_M), \quad H_M = \sum_i \sigma_i^x, \quad (23)$$

where $\ell = 1, \dots, p$ is the number of alternating layers defined by the user. The depth- p QAOA state is then

$$|\boldsymbol{\gamma}, \boldsymbol{\beta}\rangle = U_M(\beta_p)U_C(\gamma_p) \cdots U_M(\beta_1)U_C(\gamma_1)|\psi_0\rangle, \quad (24)$$

with parameter vectors $\boldsymbol{\gamma} = (\gamma_1, \dots, \gamma_p)$, $\boldsymbol{\beta} = (\beta_1, \dots, \beta_p)$. A classical outer-loop optimizer updates $(\boldsymbol{\gamma}, \boldsymbol{\beta})$ to minimize the objective

$$F_p(\boldsymbol{\gamma}, \boldsymbol{\beta}) := \langle \boldsymbol{\gamma}, \boldsymbol{\beta} | H_C | \boldsymbol{\gamma}, \boldsymbol{\beta} \rangle, \quad (25)$$

which is estimated from repeated measurements of the quantum circuit [3]. For each near-optimal parameter set, one runs QAOA in “sampling mode” to generate bitstrings which represent the candidate solutions. Several recent studies have significantly expanded and enhanced this basic formalism. [6,25,7,18].

Our first QAOA implementation follows the linear ramp schedules introduced in Ref. [14] to deterministically fix the hyper parameters $(\gamma_\ell, \beta_\ell)$ in Eq. (24) and avoid the classical parameter optimization overhead. Our second implementation follows a targeted design principle described in [18].

Linear-Ramp QAOA (LR-QAOA) In the standard formalism, the parameter vector $(\boldsymbol{\gamma}, \boldsymbol{\beta})$ of a depth- p QAOA circuit in Eq. (24) has $2p$ free angles. In Linear-Ramp QAOA (LR-QAOA), the parameter vector is reduced to two *ramp parameters* $\Delta\gamma, \Delta\beta$ by imposing a linear schedule over the layers [14],

$$\gamma_\ell = \frac{\ell}{p} \Delta\gamma, \quad \beta_\ell = \frac{p+1-\ell}{p} \Delta\beta, \quad \ell = 1, \dots, p. \quad (26)$$

The cost angle is ramped up linearly while the mixer angle is ramped down linearly, in direct analogy with a discretized annealing schedule. The depth- p LR-QAOA state is still given by Eq. (24), but is now completely specified by the two-dimensional vector $\boldsymbol{\theta}_{\text{LR}} = (\Delta\gamma, \Delta\beta)$, independent of p .

with a discretised adiabatic path.

In our implementation, for a fixed depth p , we estimate the expected energy $F_p(\Delta\gamma, \Delta\beta)$ (Eq. (25)) by sampling the circuit generated by the schedule (Eq.

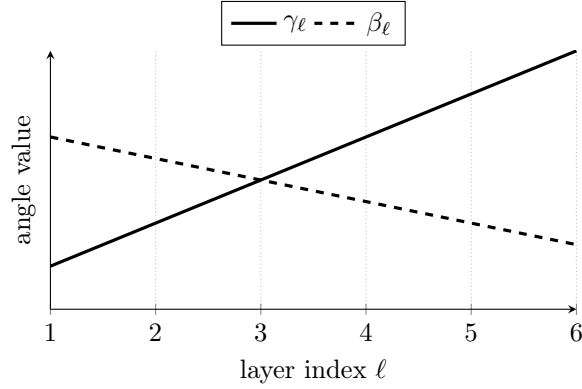


Fig. 4: Schematic linear-ramp QAOA schedule. The cost angles γ_ℓ increase linearly with the layer index ℓ while the mixer angles β_ℓ decrease linearly without instance-specific angle optimization.

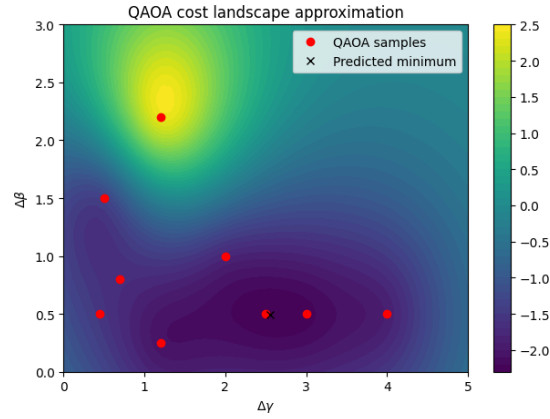


Fig. 5: QAOA cost landscape approximation for the linear-ramp schedule. The contour plot shows the Gaussian-process surrogate of the depth- p objective $F_p(\Delta\gamma, \Delta\beta)$ over the two ramp parameters. Red markers indicate the QAOA evaluations used to train the surrogate, while the black cross marks the predicted minimum $(\Delta\gamma^*, \Delta\beta^*)$ that defines the final linear schedule.

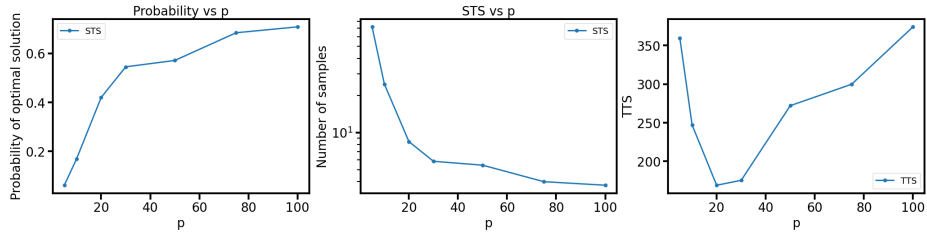


Fig. 6: Linear-ramp QAOA performance as a function of circuit depth p for a 4×4 instance (four surfers matched to four breakers). Left: single-shot success probability p_{succ} increases roughly monotonically with p , as expected from a more adiabatic schedule. Middle: samples-to-solution (STS) on a log scale drops by more than an order of magnitude before saturating, indicating improved sample efficiency at larger depth. Right: time-to-solution (TTS) shows a broad plateau, suggesting that beyond moderate depths additional layers do not pay off in wall-clock time even though p_{succ} continues to improve.

(26)). A Gaussian-process Bayesian optimizer over $(\Delta\gamma, \Delta\beta)$ is then used to locate a good minimum of F_p on a coarse grid. The resulting $(\Delta\gamma^*, \Delta\beta^*)$ are kept fixed for all subsequent sampling runs on that instance. This reduces the classical optimization overhead from a $2p$ -dimensional search to a two-dimensional calibration problem, while preserving a hardware-efficient layered circuit compatible with gate-based superconducting devices.

LR-QAOA reduces much of the heuristic “guesswork” in variational quantum optimization and yields a hardware-friendly protocol whose complexity is controlled almost entirely by the achievable depth and coherence time. As devices support larger p , the same scheduling rule extends seamlessly to deeper circuits, making LR-QAOA an attractive baseline for large-scale, low-tuning quantum optimization. At the same time, because the schedule is expressed in a low-dimensional family of ramps, it remains compatible with warm-starting and parameter-transfer strategies [15]. Precomputed QAOA parameters (e.g. from small instances, mean-field limits, or from single layer QAOA which is classically solvable [16,17]) can be distilled into effective ramp slopes and offsets, allowing LR-QAOA to inherit benefits from the broader theory of QAOA parameter transfer while keeping the on-device optimization overhead minimal.

Constraint Enhanced QAOA (CE-QAOA) Our second QAOA variant is the Constraint Enhanced QAOA introduced in [18]. It follows the general problem-algorithm co-design principles to build the quantum algorithm around the problem structure. An adaptation to the two-vehicle matching problem is as follows: let S be the number of surfers and B be the number of breakers. We group qubits into blocks such that each block has S qubits and we have B blocks in total. The total number of qubits to encode the problem remains the same ($S \cdot B$) as in the previous implementation [20]. However, in this case, a dedicated

mixer and initial state is defined over each block such that each block provides a single assignment possibility. The overall synchronization to maintain feasibility is enforced by the breaker uniqueness constraint in the diagonal Hamiltonian. Precisely, on each block we define,

$$\begin{aligned} \tilde{H}_{XY} &:= \frac{1}{S-1} \sum_{a < b} (X_a X_b + Y_a Y_b), & U_M(\beta) &= \bigotimes_{b=1}^B e^{-i\beta \tilde{H}_{XY}^{(b)}}, \\ \text{and } |s_0\rangle &= |s_{\text{blk}}\rangle^{\otimes B} \text{ with } |s_{\text{blk}}\rangle = \frac{1}{\sqrt{S}} \sum_{j=1}^S |e_j\rangle. \end{aligned} \quad (27)$$

The problem Hamiltonian is the same as in Eq. (10) and the samples generated from the quantum measurements in the computational basis are passed through a classical checker that returns the best feasible solution. The algorithm has feasibility guarantee built in [18,21]. The classical parameter optimization is replaced by a finite grid search whose resolution is defined by B . A running example of $S = B = 4$ circuit is exhibited in Fig 7. Figs. 3 and 8 summarizes the empirical performance of a single layer of CE-QAOA across all instances relative to other samplers studied in this work.

Note: We simulated CE-QAOA circuits for instance sizes ranging from $n = 3$ vehicle pairs ($N = n^2 = 9$ qubits) up to $n = 12$ vehicle pairs ($N = 144$ qubits). To keep the state-vector simulation tractable at these widths, we used the Aer `matrix_product_state` backend with MPS truncation enabled (`matrix_product_state_max_bond_dimension=128` and truncation/validation thresholds of 10^{-3}). For each parameter setting, the circuit was sampled to produce bitstrings, which were then post-processed classically. Samples were filtered by the permutation-matrix feasibility constraints and the feasible subset was evaluated under the same objective/Ising energy to report the best feasible sample returned by the quantum run.

2.8 A Digression on local trapping.

While the Tabu/SA/Leap solvers produced feasible samples for most problem sizes, we observed a pathological trapping behavior for the instance with $n = 4$. In this case, a run with $N_{\text{reads}} = 320$ returned only two unique bitstrings and *no* feasible samples (i.e., $\hat{p}_{\text{feas}} = 0$), so the empirical success probability was necessarily $\hat{p}_{\text{succ}} = 0$ under our definition (success requires feasibility and optimality within tolerance). This indicates that the Tabu dynamics became confined to a very small region of the unconstrained hypercube and failed to reach the permutation manifold (row/column one-hot constraints) at all. By contrast, for $n \in \{3, 5, 6, \dots\}$ the same implementation, typically generated feasible samples in every read, often with low diversity (e.g., a single unique feasible bitstring repeated), suggesting that once a feasible basin is entered the heuristic can remain trapped there as well.

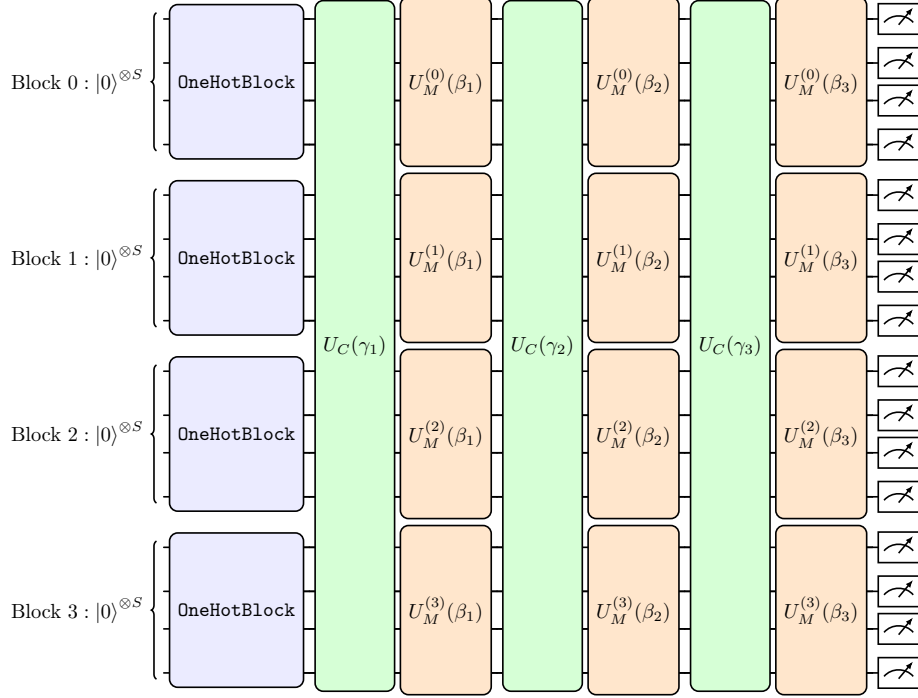


Fig. 7: Depth- $p = 3$ CE-QAOA for $B = 4$ blocks of $S = 4$ qubits (total $SB = 16$ qubits). Each block corresponds to one breaker and encodes a one-hot superposition $|s_{\text{blk}}\rangle$ over the S surfer indices prepared by `OneHotBlock`, so that the global initial state is $|s_0\rangle = |s_{\text{blk}}\rangle^{\otimes B}$. Each layer applies a global cost unitary $U_C(\gamma_\ell) = e^{-i\gamma_\ell H_C}$ over all SB wires, followed by parallel block-local XY mixers $U_M^{(b)}(\beta_\ell) = \exp[-i\beta_\ell \tilde{H}_{XY}^{(b)}]$ on each block $b = 0, 1, 2, 3$, with $\tilde{H}_{XY} = \frac{1}{S-1} \sum_{a < b} (X_a X_b + Y_a Y_b)$.

We further found that increasing the penalty scaling parameter λ_3 can force the Tabu heuristic to produce feasible assignments for $n = 4$, but at the cost of yielding systematically suboptimal objective values, consistent with an overly strong penalty dominating the effective energy landscape. Notably, the theoretically-motivated scaling used throughout this work produced stable behavior across the remaining instances, which suggests that the $n = 4$ failure mode is more likely attributable to heuristic initialization and/or Tabu hyperparameters (e.g., initial state, tenure, or neighborhood/aspiration settings) than to a fundamental issue with the formulation. Since Tabu Search is used here purely as a reference heuristic and comprehensive hyperparameter optimization is not the focus of this paper, we leave a systematic parameter and restart study (including multi-start initialization strategies) for future work.

3 Evaluating Practical Benefits

Optimizing Windbreaking-as-a-Service (WaaS) is meaningful only if the binary decisions inside the QUBO translate into transparent physical benefits like CO₂ emission reduction, EV-range extension, and charger relief. For a windsurfer of class c_s drafting behind a breaker of class, C_b the slip-stream efficiency is modeled as the linear map [1,20]

$$f(d) = \frac{d+4}{24}, \quad d := C_b - c_s \in \{-4, \dots, 4\}, \quad (28)$$

so that $f(-4) = 0$ (tiny breaker, large surfer) and $f(4) = \frac{1}{3}$ (best pairing: large breaker, small surfer).

The surfer classes are defined such that an individual vehicle's aerodynamic drag coefficient is (roughly) proportional to the class c_s it belongs to. Therefore, if a surfer s is traversing a certain motorway edge at the breaker's speed V_b , the associated aerodynamic *energy per unit distance* is

$$E_{s,b} = c_s V_b^2 [1 - f(C_b - c_s)]. \quad (29)$$

To minimize the aerodynamic drag energy and, by extension, CO₂ emissions or battery discharge, we track *four* cost functions outlined below (also summarized in Table 1).

1 — *Solo driving at preferred speed.* The *reference cost*

$$F_{\text{ref}} = \sum_{s=1}^S c_s v_s^2 \quad (30)$$

assumes every windsurfer drives alone at their own cruise speed v_s . All subsequent energies are reported *relative* to F_{ref}

2 — *Velocity-corrected reference.* The problem setup is such that the surfers are forced to follow the breakers at their speed $V_b \neq v_s$. The hypothetical cost of solo vehicle driving at corrected velocity V_b is

$$F_{\text{ref}}^{\text{vel}} = \sum_{s=1}^S c_s V_b^2. \quad (31)$$

Comparing $F_{\text{ref}}^{\text{vel}}$ with F_{ref} *isolates* the energetic penalty (or gain) is due purely to imposed speed changes and is crucial when the optimizer produces very slow or very fast convoys.

3 — *Objective part of the cost minimized by the optimizer* The matching problem minimizes

$$F_1 = \sum_{s=1}^S c_s V_b^2 [1 - f(C_b - c_s)], \quad (32)$$

i.e. aerodynamic energy with the breaker speed and the slipstream efficiency from Eq. (28) with every computed pairing accepted.

4 — *Post Optimization: modified objective* After optimization we re-evaluate the schedule: any surfer whose timing or velocity constraints are still violated simply *opts out* and keeps driving alone at v_s . Splitting the index set into “assigned” surfers A and “unassigned” surfers U gives

$$F_1^{\text{mod}} = \sum_{s \in A} c_s V_b^2 [1 - f(C_b - c_s)] + \sum_{s \in U} c_s v_s^2. \quad (33)$$

The gap $F_1^{\text{mod}} - F_{\text{ref}}$ therefore measures the *realizable* drag saving once human acceptance is considered.

Table 1: Hierarchy of cost functions.

Name	Informal meaning	Eq.#
F_{ref}	Every surfer drives <i>solo</i> at their own preferred speed v_s ; no windbreaking.	(30)
$F_{\text{ref}}^{\text{vel}}$	Still solo, but forced to adopt the <i>speed profile implied by the optimizer</i> (typically the leader’s speed). Isolates the pure “speed-change” penalty or gain.	(31)
F_1	The optimizer’s aerodynamic energy using pairing rule and breaker speed, but <i>ignoring unmet preferences</i> . This is the objective actually minimized in the QUBO/MIQP.	
F_1^{mod}	Post-hoc correction: surfers whose constraints are violated abandon the match and revert to solo driving at v_s . Gives a realistic <i>ex-post</i> energy once humans are allowed to veto bad pairings.	(33)

The percentage energy change relative to the preferred-speed baseline F_{ref} as

$$\eta_{\text{speed}} := 100 \frac{F_{\text{ref}} - F_{\text{ref}}^{\text{vel}}}{F_{\text{ref}}}, \quad (34)$$

$$\eta_{F_1} := 100 \frac{F_{\text{ref}} - F_1}{F_{\text{ref}}}, \quad (35)$$

$$\eta_{F_1^{\text{mod}}} := 100 \frac{F_{\text{ref}} - F_1^{\text{mod}}}{F_{\text{ref}}}. \quad (36)$$

A positive η indicates an energy saving relative to F_{ref} , while a negative value indicates an energy increase.

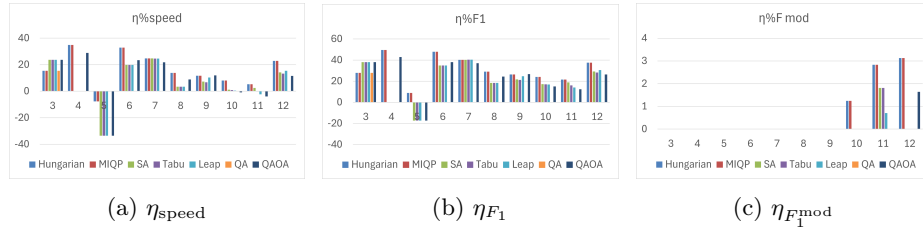


Fig. 8: Comparison of percentage savings metrics relative to F_{ref} . Negative values in η_{speed} and η_{F_1} can occur when an assignment forces a surfer to drive faster than their preferred speed ($V_b > v_s$), so the quadratic speed scaling increases energy enough to outweigh slipstream gains and yields worse-than-solo performance. The post-optimization veto used in F_1^{mod} removes this pathology by letting surfers reject such undesirable pairings and revert to solo driving at v_s , so $\eta_{F_1^{\text{mod}}}$ reflects realizable savings under human acceptance. See the underlying tables in the Supplementary Material in App. A.

4 Conclusion

We studied the two-vehicle matching subproblem behind Windbreaking-as-a-Service (WaaS) and cast it into a linear assignment formulation with an equivalent QUBO/Ising representation. This allowed us to benchmark a heterogeneous “solver zoo” including exact classical baselines (Hungarian, MIQP), classical meta-heuristics (SA, Tabu), and quantum / quantum-inspired approaches (quantum annealing, Leap Hybrid, gate-model QAOA). The main practical takeaway is that the QUBO acts as a *lingua franca* that lets fundamentally different backends attack the same high-order landscape and makes solver comparisons meaningful via shared solver agnostic metrics.

Across the tested instances, the exact baselines provide ground-truth labels and confirm correctness of the encodings. Among heuristic methods, we observed that feasibility is not automatic in the unconstrained hypercube and depends sensitively on penalty scaling and solver dynamics. This motivates constraint-aware quantum design like CE-QAOA which enforces row-wise one-hot structure by construction and shifts the burden to a smaller set of remaining constraints plus a classical feasibility checker. Even at shallow depth ($p = 1$), this structured approach is observed to yield non-trivial success probabilities, illustrating why problem-aware encodings can matter more than simply increasing circuit depth in generic QAOA. On the other hand, LR-QAOA mitigates the parameter-tuning bottleneck of quantum heuristics by replacing the unstable $2p$ -angle search with a fixed monotone schedule, making depth p the main control knob. Figure 6 shows that this yields a well-behaved scaling where p_{succ} increases with p and STS falls dramatically, so deeper circuits translate directly into higher hit-rate without the confounder of optimizer convergence. The early TTS plateau then identifies a practical depth window where added layers still

improve success probability but no longer buy wall-clock speedups, separating algorithmic gains from hardware overhead.

Data Availability

All data and Python implementation are available at: <https://doi.org/10.5281/zenodo.17768136> [19].

Conflict of Interests

All authors declare no competing interests.

Author contributions

All authors contributed equally. In addition, Carsten Othmer and Kristel Michielsen provided guidance during the project. All the authors reviewed the paper.

Funding

This research received no external funding.

Correspondence and requests for materials should be addressed to Chinonso Onah (chinonso.calistus.onah@volkswagen.de).

References

1. Alam, A., Besselink, B., Turri, V., Mårtensson, J., Johansson, K. H.: Heavy-duty vehicle platooning for sustainable freight transportation: A review. *IEEE Control Systems Magazine* **35**(6), 34–56 (2015)
2. Albash, T., Lidar, D. A.: Adiabatic quantum computation. *Reviews of Modern Physics* **90**(1), 015002 (2018)
3. Farhi, E., Goldstone, J., Gutmann, S.: A quantum approximate optimization algorithm (2014), [quant-ph]
4. Geman, S., Geman, D.: Stochastic relaxation, gibbs distributions, and the Bayesian restoration of images. *IEEE Transactions on Pattern Analysis and Machine Intelligence* **PAMI-6**, 721–741 (1984), (6)
5. Glover, F.: Future paths for integer programming and links to artificial intelligence. *Computers & Operations Research* **13**(5), 533–549 (1986)
6. Hadfield, S., Wang, Z., O’Gorman, B., et al.: From the quantum approximate optimization algorithm to a quantum alternating operator ansatz. *Algorithms* **12**(2), 34 (2019)
7. Harwood, S., Gambella, C., Tenev, D., Simonetto, A., Bernal, D., Greenberg, D.: Formulating and solving routing problems on quantum computers. *IEEE transactions on quantum engineering* **2**, 1–17 (2021)

8. Inc, D.W.S.: Leap service’s hybrid solvers documentation. (accessed 2025), <https://docs.dwavequantum.com>
9. Kadowaki, T., Nishimori, H.: Quantum annealing in the transverse ising model. *Physical Review E* **58**(5), 5355–5363 (1998)
10. Kirkpatrick, S., Gelatt, C. D., Vecchi, M. P.: Optimization by simulated annealing. *Science* **220**(4598), 671–680 (1983)
11. Kuhn, H. W.: The hungarian method for the assignment problem. *Naval Research Logistics Quarterly* **2**(1-2), 83–97 (1955)
12. Lucas, A.: Ising formulations of many np problems. *Frontiers in physics* **2**, 5 (2014)
13. McGeoch, C. C.: *Adiabatic Quantum Computation and Quantum Annealing: Theory and Practice*. Synthesis Lectures on Quantum Computing. Morgan & Claypool, San Rafael (2014)
14. Montanez-Barrera, J., Michielsen, K.: Towards a universal qaoa protocol: Evidence of a scaling advantage in solving some combinatorial optimization problems. arXiv 2024. arXiv preprint arXiv:2405.09169 (2024)
15. Montañez-Barrera, J.A., Willsch, D., Michielsen, K.: Transfer learning of optimal qaoa parameters in combinatorial optimization (2024), arXiv preprint
16. Onah, C., Michielsen, K.: Scalable hardware maturity probe for quantum accelerators via harmonic analysis of qaoa (2025), [quant-ph]
17. Onah, C.: Single-layer qaoa p = 1 global-optimum catalogue (v1.0) (2025). <https://doi.org/10.5281/ZENODO.15878141>, <https://zenodo.org/doi/10.5281/zenodo.15878141>
18. Onah, C., Firt, R., Michielsen, K.: Empirical quantum advantage in constrained optimization from encoded unitary designs. arXiv preprint arXiv:2511.14296 (2025)
19. Onah, C., Guin, A., Montanez Barrera, A., Othmer, C., Michielsen, K.: Dataset for quantum and classical approaches to the optimisation of highway platooning: the two-vehicle matching problem (2025). <https://doi.org/10.5281/ZENODO.17768136>, <https://zenodo.org/doi/10.5281/zenodo.17768136>
20. Onah, C., Misciasci, N., Othmer, C., Michielsen, K.: Quest: Quantum-enhanced shared transportation. In: 2025 IEEE International Conference on Quantum Computing and Engineering (QCE). vol. 1, pp. 2149–2160. IEEE (2025)
21. Onah, C., Roman, F., Michielsen, K.: Dataset: Empirical quantum advantage in constrained optimization from encoded unitary designs (2025). <https://doi.org/10.5281/ZENODO.15725265>, <https://zenodo.org/doi/10.5281/zenodo.15725265>
22. Optimization, G., Gurobi, L.: *Optimizer reference manual* (2024), <https://www.gurobi.com>
23. Rønnow, T. F., Wang, Z., Job, J., et al.: Defining and detecting quantum speedup. *Science* **345**(6195), 420–424 (2014)
24. Vert, D., Sirdey, R., Louise, S.: Benchmarking quantum annealing against “hard” instances of the bipartite matching problem. *SN Computer Science* **2**, 133 (2021)
25. Zhou, L., Wang, S.T., Choi, S., Pichler, H., Lukin, M. D.: Quantum approximate optimization algorithm: Performance, mechanism, and implementation on near-term devices. *Physical Review X* **10**(2), 021067 (2020)

A Supplementary Material.

We provide the benchmarking tables supporting the solver-zoo results in the main text. For each instance size $n \in \{3, \dots, 12\}$ and each solver, the supplement reports the raw and derived metrics used in our comparisons (best/mean energy, gaps to the exact baseline E_* , success probability, STS/TTS, feasibility counts, and wall time), as well as energy-savings tables that map matchings to F_{ref} , $F_{\text{ref}}^{\text{vel}}$, F_1 , F_1^{mod} and the corresponding η -metrics. These tables serve as a reproducible audit trail and allow readers to reconstruct every plotted summary statistic.

A.1 Solver Comparison Tables

Here we report the polynomial-time Hungarian assignment baseline on the same $n \times n$ surfer-breaker matching instances as the heuristic solvers. As an exact algorithm, the Hungarian solver always returns a feasible match with $p_{\text{feas}} = p_{\text{succ}} = 1$, vanishing optimality gaps, and zero energy variance. The wall-clock time remains essentially negligible across $n = 3, \dots, 12$ compared to MIQP and all heuristic quantum and classical samplers. For the heuristics, we report the total number of reads (N_{reads}), number of unique samples (N_{unique}), feasible counts in reads/unique ($n_{\text{feas}}^{\text{reads}}, n_{\text{feas}}^{\text{unique}}$), exact and tolerance-based success counts ($n_{\text{succ,exact}}, n_{\text{succ,tol}}$), feasibility and success probabilities ($p_{\text{feas}}, p_{\text{succ,exact}}, p_{\text{succ,tol}}$), samples-to-solution (STS), time-to-solution (TTS), internal evaluation proxy (N_{eval}), wall time, and energy statistics relative to the ground state E_* .

Table 2: Hungarian and Gurobi MIQP

Table (a): Hungarian assignment baseline metrics for the WaaS instances with $n = 3, \dots, 12$.

SOLVER	n	E_*	E_{best}	E_{mean}	p_{succ}	STS	TTS [s]	gap	best_gap	mean	$\sigma_{\bar{E}}$	wall_time	-	-
Hungarian	3	289224.42	289224.42	289224.42	0	0	0	1	1	1	0	0	-	-
	4	236096.63	236096.63	236096.63	0	0	0	1	1	1	0	0	-	-
	5	415103.38	415103.38	415103.38	0	0	0	1	1	1	0	0	-	-
	6	486510	486510	486510	0	0	0	1	1	1	0	0	-	-
	7	511283.17	511283.17	511283.17	0	0	0	1	1	1	0	0	-	-
	8	532659.67	532659.67	532659.67	0	0	0	1	1	1	0	0	-	-
	9	485653.17	485653.17	485653.17	0	0	0	1	1	1	0	0	-	-
	10	578870.88	578870.88	578870.88	0	0	0	1	1	1	0	0	-	-
	11	722931.75	722931.75	722931.75	0	0	0	1	1	1	0	0	-	-
	12	761017.5	761017.5	761017.5	0	0	0	1	1	1	0	0	-	-

Table (b): Gurobi MIQP baseline metrics for the surfer-breaker matching instances with $n = 3, \dots, 12$.

SOLVER	n	E_*	E_{best}	E_{mean}	p_{succ}	STS	TTS [s]	gap	best_gap	mean	$\sigma_{\bar{E}}$	wall_time	\bar{E}_{LB}	miqp_gap
Gurobi-MIQP	3	-664153	-664153	-664153	0	0	0	1	1	0.0061329	0.00613291	0.00613291	-664153	0
	4	-705978	-705978	-705978	0	0	0	1	1	0.0038813	0.00388131	0.00388131	-705978	0
	5	-3.84E+06	-3.84E+06	-3.84E+06	0	0	0	1	1	0.0043231	0.00432311	0.00432311	-3.84E+06	0
	6	-3.38E+06	-3.38E+06	-3.38E+06	0	0	0	1	1	0.00586	0.00586001	0.00586001	-3.38E+06	0
	7	-5.91E+06	-5.91E+06	-5.91E+06	0	0	0	1	1	0.008417	0.00841702	0.00841702	-5.91E+06	0
	8	-7.95E+06	-7.95E+06	-7.95E+06	0	0	0	1	1	0.0112449	0.0112449	0.0112449	-7.95E+06	0
	9	-1.01E+07	-1.01E+07	-1.01E+07	0	0	0	1	1	0.434102	0.434102	0.434102	-1.01E+07	0
	10	-1.28E+07	-1.28E+07	-1.28E+07	0	0	0	1	1	0.755872	0.755872	0.755872	-1.28E+07	0
	11	-2.19E+07	-2.19E+07	-2.19E+07	0	0	0	1	1	1	1	1	-2.19E+07	0
	12	-2.61E+07	-2.61E+07	-2.61E+07	0	0	0	1	1	3	3	3	-2.61E+07	3.83E-05

Table 3: Simulated Annealing and Tabu Search

Table (a): Simulated annealing (SA) benchmarking summary on the surfer-breaker QUBO instances with $n = 3, \dots, 12$.

SOLVER	n	E^*	E_{best}	E_{mean}	P_{succ}	total STS	tot TTS	$ s $	gap	best gap	mean	σ^2	wall_time	$ s $	N_{reads}	N_{unique}	n_{reads}	n_{feas}	n_{succ}	$n_{\text{succ,exact}}$	$n_{\text{succ,tot}}$	$n_{\text{succ,unique}}$	P_{succ}	$P_{\text{succ,exact}}$	
SA	3	-664153	-664153	-642098	2.51E-06	3.32083	2.65E+08	0.275556	0	0.275556	3.62903	0.260133	0.260133	1350	6	1350	6	372	1	1	1	1	1	0.275556	0
	4	-705978	-696790	-678267	1.30152	3.92522	2.47E+08	0	∞	1.11575	∞	1.11575	3200	51	2013	24	0	0	0	0	0	0	0	0.629062	0
	5	-3.84E+06	-3.84E+06	-3.73E+06	8.69E-06	2.78552	4.60E+09	0.0424	23.5849	3.54369	3.54369	3.54369	6250	120	6250	120	140	1	265	2	1	1	1	0.0224	0
	6	-3.38E+06	-3.38E+06	-3.29E+06	-8.14E-06	2.77748	4.64E+09	0.013611	73.4694	8.47563	8.47563	8.47563	10800	721	10799	720	101	2	147	3	0.999907	0.999907	0.999907	0.009352	0
	7	-5.91E+06	-5.91E+06	-5.73E+06	3.25E-06	2.65654	4.80E+09	0.001516	659.615	3.30959	3.30959	3.30959	17150	4600	17150	4600	26	2	26	2	1	1	1	0.001516	0
	8	-7.95E+06	-7.95E+06	-7.73E+06	7.33E-07	2.84316	8.72E+09	0.000664	1505.88	10.1422	37.4525	25600	17308	25600	17308	3	1	17	5	1	1	1	1	0.000117	0
	9	-1.01E+07	-1.01E+07	-9.88E+06	-2.33E-05	2.49217	8.71E+09	0.000466	2144.12	18.0282	68.7822	36450	34158	36450	34158	4	4	17	13	1	1	1	1	0.00011	0
	10	-1.28E+07	-1.28E+07	-1.25E+07	-2.30E-05	2.97453	1.53E+10	4.00E-05	25000	277.34	120.45	50000	49484	50000	49484	2	2	2	2	1	1	1	1	4.00E-05	0
	11	-2.20E+07	-2.19E+07	-2.14E+07	0.194748	2.51915	2.06E+10	0	∞	∞	198.022	66550	66471	66550	66471	0	0	0	0	0	0	0	0	1	0
	12	-2.61E+07	-2.61E+07	-2.56E+07	0.0759048	2.11518	2.54E+10	1.16E-05	86400	1.41756	307.821	86400	86386	86400	86386	0	0	1	1	1	1	1	1	1	0

Table (b): Tabu search baseline metrics for the surfer-breaker matching instances with $n = 3, \dots, 12$.

SOLVER	n	E^*	E_{best}	E_{mean}	P_{succ}	total STS	tot TTS	$ s $	gap	best gap	mean	σ^2	wall_time	$ s $	N_{reads}	N_{unique}	n_{reads}	n_{feas}	n_{succ}	$n_{\text{succ,exact}}$	$n_{\text{succ,tot}}$	$n_{\text{succ,unique}}$	P_{succ}	$P_{\text{succ,exact}}$	
TABU	3	-664153	-664153	-664153	2.51E-06	2.51E-06	1.36E-20	1	1	1	28.3509	∞	28.3509	1350	1	1350	1	1350	1	1	1	1	1	1	1
	4	-705978	-	-	8.69E-06	8.69E-06	8.67E-19	1	1	1	131.26	∞	67.2024	3200	2	0	0	0	0	0	0	0	0	0	0
	5	-3.84E+06	-3.84E+06	-3.84E+06	-8.14E-06	-8.14E-06	2.17E-19	1	1	1	226.811	131.26	131.26	6250	1	6250	1	6250	1	6250	1	1	1	1	1
	6	-3.38E+06	-3.38E+06	-3.38E+06	-5.90E+06	-5.90E+06	0.051874	2.33E+07	0.677668	1.47565	360.176	226.811	226.811	10800	2	10800	2	10800	2	10800	2	10800	2	1	1
	7	-5.91E+06	-5.91E+06	-5.90E+06	-7.95E+06	-7.95E+06	0.0294433	5.78E+06	0.977539	1.02298	537.657	360.176	360.176	17150	30	17150	30	11622	2	11622	2	1	1	0.677668	0
	8	-7.95E+06	-7.95E+06	-7.95E+06	-1.01E+07	-1.01E+07	0.337737	3.07E+08	0.122222	8.18182	765.553	537.657	537.657	25600	19	25600	19	11972	1	25025	6	1	1	0.467656	0
	9	-1.01E+07	-1.01E+07	-1.01E+07	-1.28E+07	-1.28E+07	0.173814	1.55E+08	0.23528	4.25026	1050.19	765.553	765.553	36450	1850	36450	1850	831	4	4455	18	1	1	0.022798	0
	10	-1.28E+07	-1.28E+07	-1.28E+07	-2.19E+07	-2.19E+07	0.175365	3.08E+08	0.177295	5.64031	1397.87	1050.19	1050.19	50000	440	50000	440	2405	2	11764	11	1	1	0.0481	0
	11	-2.20E+07	-2.19E+07	-2.19E+07	-2.61E+07	-2.61E+07	0.129737	1.46E+08	0.27015	3.70164	1814.92	1397.87	1397.87	66550	648	66550	648	1111	1	11799	10	1	1	0.016694	0
	12	-2.61E+07	-2.61E+07	-2.61E+07	-	-	0.129737	1.46E+08	0.27015	3.70164	1814.92	1814.92	1814.92	86400	4320	86400	4320	15	2	23341	315	1	1	0.000174	0

Table 4: Leap hybrid Solver, QPU-QA and CE-QAOA

SOLVER	n	E_s	E_{best}	E_{mean}	E_{max}	P_{succ}	STS	TTS [s]	gap_best	gap_mean	σ_s^2	wall_time [s]
LEAP	3	-664153.2	-6.64E+05	-6.64E+05	0.000003	0.000003	0	1	1	2.544257	2.544257	2.40487
	4	-705978.4	-7.06E+05	-7.06E+05	0.000002	0.000002	0	1	1	2.40487	2.40487	2.537564
	5	-383591.4	-3.84E+06	-3.84E+06	0.000009	0.000009	0	1	1	2.537564	2.537564	2.446772
	6	-337937.1	-3.38E+06	-3.38E+06	-0.000008	-0.000008	0	1	1	2.446772	2.446772	2.405447
	7	-590568.5	-5.91E+06	-5.91E+06	0.000003	0.000003	0	1	1	2.405447	2.405447	2.519187
	8	-795342.1	-7.95E+06	-7.95E+06	0.075439	0.075439	0	1	1	2.519187	2.519187	2.521728
	9	-1013060.0	-1.01E+07	-1.01E+07	0.273869	0.273869	0	1	1	2.521728	2.521728	2.548852
	10	-1284774.0	-1.28E+07	-1.28E+07	0.378651	0.378651	0	1	1	2.548852	2.548852	2.574582
	11	-2194960.0	-2.19E+07	-2.19E+07	1.02324	1.02324	0	1	1	2.574582	2.574582	2.523256
	12	-26125560.0	-2.61E+07	-2.61E+07	0.519158	0.519158	0	1	1	2.523256	2.523256	

SOLVER	n	E_s	E_{best}	E_{mean}	E_{max}	P_{succ}	STS	TTS [s]	gap_best	gap_mean	σ_s^2	wall_time [s]
QPU-QA	3	-664153.2	-664153.2	-4.76E+07	-2.27E-07		0.718004	1.66E+11	0.013333	75	0.06907	0.002249
	4	-	-	-	-	-	-	-	-	-	-	-
	5	-	-	-	-	-	-	-	-	-	-	-
	6	-	-	-	-	-	-	-	-	-	-	-
	7	-	-	-	-	-	-	-	-	-	-	-
	8	-	-	-	-	-	-	-	-	-	-	-
	9	-	-	-	-	-	-	-	-	-	-	-
	10	-	-	-	-	-	-	-	-	-	-	-
	11	-	-	-	-	-	-	-	-	-	-	-
	12	-	-	-	-	-	-	-	-	-	-	-

SOLVER	n	E_s	E_{best}	E_{mean}	E_{max}	P_{succ}	STS	TTS [s]	gap_best	gap_mean	σ_s^2	wall_time [s]	β_{best}	β_{grid}	evals
CE-QAOA $p=1$	3	-664153.1833	-664153.1833	-637137.1885	0.000493827	2025	0.8439542405000111	0	3.8949822024248126	9701735.127624512	1.6879084810000222	1.215	0.65	1	
	4	-696789.9833	-696789.9833	-662714.1625	0.006171875	162.02531645569618	0.018429363	0	4.255877841421934	442787449.34717173	1.455919659000017	2.375	0.779	1	
	5	-383591.3667	-383591.3667	-3695132.661	0.000512	1953.125	0.3637791215625015	0	3.7033476397929923	54732579.517578	5.820465945000024	2.36	2.327	1	
	6	-337937.1275	-337937.1275	-3237746.234	0	0	0	0.037186404345927945	3.7659176601021156	44.0013620529297	36.28281790699998	2.068	0.497	1	
	7	-590568.4808	-5876006.725	-5710483.383	0	0	0	0.2539925594882839	3.731117242778161	5301.543150.589844	92.18202271	2.795	0.543	1	
	8	-795342.1058	-7936565.392	-7667142.702	0	0	0	0.21192976636104913	3.5994366993384954	9398836487.789062	100.82788856100001	1.626	2.51	1	
	9	-1013060.236	-10056341.69	-9837173.529	0	0	0	0.7330330817456795	2.8904060213858178	836494257.2546875	430.85198196500005	0.16	2.295	1	
	10	-1284774.296	-12637655.96	-12357610.94	0	0	0	1.6320505904026057	3.814927053246903	19198801547.03125	401.4604331	1.417	0.804	1	
	11	-2194949.89	-21773245.06	-21336791.99	0	0	0	0.805035247	2.7934364522101824	21793378311	645.0540156	2.35	0.804	1	
	12	-26125560.03	-25828688.19	-25504276.7	0	0	0	1.1363271564273298	2.3780670286065773	28172280925	984.7312200189999	1.829	0.822	1	

Table (a): Leap hybrid solver baseline metrics for the surfer-breaker matching instances with $n = 3, \dots, 12$.Table (b): Quantum annealing (QPU-QA) baseline metrics for the surfer-breaker matching instances with $n = 3, \dots, 12$.Table (c): CE-QAOA $p=1$ baseline metrics for the surfer-breaker matching instances with $n = 3, \dots, 12$.

A.2 Energy Savings

Energy benchmarks for the various solvers across problem sizes $n = 3, \dots, 12$ are given in Tables 5, 7 and 6. For each instance size n we report the reference solo fuel cost at the surfers' preferred speeds F_{ref} , the solo cost at the breakers' speeds $F_{\text{ref,vel}}$, the paired aerodynamic cost F_1 , the post-hoc corrected cost $F_{1,\text{mod}}$, the relative speed efficiency η_{speed} , and the relative fuel efficiencies η_{F_1} and $\eta_{F_{1,\text{mod}}}$ (all in %). The relative speed efficiency η_{speed} measures the average deviation in speed between the paired solution and the solo reference (in percent), whereas η_{F_1} and $\eta_{F_{1,\text{mod}}}$ measure the relative fuel savings of the paired solution with respect to F_{ref} .

Table 5: Hungarian baseline evaluation of the four aerodynamic cost functions for single-segment surfer–breaker matching instances with $n = 3, \dots, 12$ vehicles.

solver	n	F_{ref}	$F_{\text{ref}}^{\text{vel}}$	F_1	F_1^{mod}	$\eta_{\text{speed}}^{\%}$	$\eta_{F_1}^{\%}$	$\eta_{F_1^{\text{mod}}}^{\%}$
Hungarian	3	118196	99965	85224.4	118196	15.4244	27.8957	0
	4	118848	77313	59872.4	118848	34.948	49.6227	0
	5	177451	191125	161813	177451	-7.70579	8.81257	0
	6	191983	128938	100139	191983	32.8388	47.8396	0
	7	250936	188828	150047	250936	24.7505	40.2049	0
	8	319735	275579	227127	319735	13.8102	28.9639	0
	9	386078	340914	284404	386078	11.6982	26.3351	0
	10	408253	375535	310364	403168	8.01415	23.9776	1.24563
	11	460393	435895	361098	447370	5.32111	21.5674	2.82874
	12	483876	373206	301902	468732	22.8716	37.6075	3.12976

Table 6: Energy Saving for MIQP, SA and Tabu search

Table (a): Fuel / energy benchmarks for the Gurobi-based MIQP assignment solver across problem sizes $n = 3, \dots, 12$.									
SOLVER	n	F_{ref}	$F_{\text{ref}}^{\text{vel}}$	F_1	F_1^{mod}	$\eta_{\text{speed}}^{\%}$	$\eta_{F_1}^{\%}$	$\eta_{F_1^{\text{mod}}}^{\%}$	wall_time [s]
MIQP	3	118196	99965	85224.4	118196	15.4244	27.8957	0	0.00320431
	4	118848	77313	59872.4	118848	34.948	49.6227	0	0.00319371
	5	177451	191125	161813	177451	-7.70579	8.81257	0	0.00418791
	6	191983	128938	100139	191983	32.8388	47.8396	0	0.00409631
	7	250936	188828	150047	250936	24.7505	40.2049	0	0.00498731
	8	319735	275579	227127	319735	13.8102	28.9639	0	0.00622701
	9	386078	340914	284404	386078	11.6982	26.3351	0	0.00897401
	10	408253	375535	310364	403168	8.01415	23.9776	1.24563	0.00887621
	11	460393	435895	361098	447370	5.32111	21.5674	2.82874	0.0109073
	12	483876	373206	301902	468732	22.8716	37.6075	3.12976	0.0131957
	Table (b): Fuel / energy benchmarks for the Simulated Annealing solver across problem sizes $n = 3, \dots, 12$.								
	SOLVER	n	F_{ref}	$F_{\text{ref}}^{\text{vel}}$	F_1	F_1^{mod}	$\eta_{\text{speed}}^{\%}$	$\eta_{F_1}^{\%}$	$\eta_{F_1^{\text{mod}}}^{\%}$
SA	3	118196	90259	73225.17	118196	23.63616	38.04768	0	0.291408
	4	—	—	—	—	—	—	—	—
	5	177451	237021	208184.5	177451	-33.56983	-17.31941	0	3.721341
	6	191983	153819	125088.5	191983	19.87884	34.84395	0	9.310699
	7	250936	188828	150047.5	250936	24.75053	40.20489	0	20.60184
	8	319735	308982	261156.2	319735	3.363098	18.32104	0	41.10357
	9	386078	358159	302137	386078	7.23144	21.74197	0	75.49417
	10	408253	403493	337932.7	408253	1.165944	17.22469	0	130.9877
	11	460393	449256	373756.5	452070.2	2.41902	18.81795	1.807767	216.8527
	12	483876	415056	342883.5	483876	14.22265	29.13815	0	339.4152
	Table (c): Fuel / energy benchmarks for the Tabu search across problem sizes $n = 3, \dots, 12$.								
	SOLVER	n	F_{ref}	$F_{\text{ref}}^{\text{vel}}$	F_1	F_1^{mod}	$\eta_{\text{speed}}^{\%}$	$\eta_{F_1}^{\%}$	$\eta_{F_1^{\text{mod}}}^{\%}$
TABU	3	118196	90259	73225.17	118196	23.63616	38.04768	0	28.35091
	4	—	—	—	—	—	—	—	—
	5	177451	237021	208184.5	177451	-33.56983	-17.31941	0	131.2603
	6	191983	153819	125088.5	191983	19.87884	34.84395	0	226.8114
	7	250936	189328	149823.5	250936	24.55128	40.29416	0	360.1759
	8	319735	308982	261156.2	319735	3.363098	18.32104	0	537.6573
	9	386078	360293	304482.8	386078	6.678702	21.13437	0	765.553
	10	408253	404429	338868.7	408253	0.9366741	16.99543	0	1050.191
	11	460393	461378	386723.4	452070.2	-0.2139476	16.00147	1.807767	1397.873
	12	483876	419391	347627.9	483876	13.32676	28.15764	0	1814.92

Table 7: Energy Saving for Leap hybrid solver, QPU-QA and CE-QAOA

Table (a): Fuel / energy benchmarks for the Leap solver across problem sizes $n = 3, \dots, 12$.										
SOLVER	n	F_{ref}	$F_{\text{ref}}^{\text{vel}}$	F_1	F_1^{mod}	$\eta_{\text{speed}}^{\%}$	$\eta_{F_1}^{\%}$	$\eta_{F_1^{\text{mod}}}^{\%}$	wall_time [s]	
LEAP	3	118196	99965	85224.4	118196	15.4244	27.8957	0.0000	0.151	
	4	—	—	—	—	—	—	—	1.201	
	5	177451	222350	192307.0	177451	-25.3022	-8.37208	0.0000	2.113	
	6	191983	152266	123548.0	191983	20.6878	35.6463	0.0000	48.211	
	7	250936	209134	170072.0	250936	16.6584	32.2251	0.0000	68.707	
	8	319735	291539	241886.0	319735	8.81855	24.3479	0.0000	3499.81	
	9	386078	349768	293105.0	386078	9.40484	24.0813	0.0000	113.664	
	10	408253	382559	316148.0	408253	6.29365	22.5607	0.0000	594.469	
	11	460393	478160	403729.0	460393	-3.85909	12.3078	0.0000	575.165	
	12	483876	383856	309568.0	457463	20.6706	36.0233	1.4586	1623.56	
	Table (b): Fuel / energy benchmarks for the QPU solver across problem sizes $n = 3, \dots, 12$.									
	SOLVER	n	F_{ref}	$F_{\text{ref}}^{\text{vel}}$	F_1	F_1^{mod}	$\eta_{\text{speed}}^{\%}$	$\eta_{F_1}^{\%}$	$\eta_{F_1^{\text{mod}}}^{\%}$	wall_time [s]
QPU-QA	3	118196	99965	85224.4	118196	15.4244	27.8957	0.0000	0.151	
	4	—	—	—	—	—	—	—	1.201	
	5	—	—	—	—	—	—	—	2.113	
	6	—	—	—	—	—	—	—	48.211	
	7	—	—	—	—	—	—	—	68.707	
	8	—	—	—	—	—	—	—	3499.81	
	9	—	—	—	—	—	—	—	113.664	
	10	—	—	—	—	—	—	—	594.469	
	11	—	—	—	—	—	—	—	575.165	
	12	—	—	—	—	—	—	—	1623.56	
	Table (c): Fuel / energy benchmarks for the CE-QAOA solver across problem sizes $n = 3, \dots, 12$.									
	SOLVER	n	F_{ref}	$F_{\text{ref}}^{\text{vel}}$	F_1	F_1^{mod}	$\eta_{\text{speed}}^{\%}$	$\eta_{F_1}^{\%}$	$\eta_{F_1^{\text{mod}}}^{\%}$	wall_time [s]
CE-QAOA	3	118196	90259	73225.17	118196.00	23.64	38.05	0.00	0.15	
	4	118848	84589	67857.75	118848.00	28.83	42.90	0.00	1.20	
	5	177451	237021	208184.46	177451.00	-33.57	-17.32	0.00	2.11	
	6	191983	135636	106395.79	191983.00	29.35	44.58	0.00	48.21	
	7	250936	188828	150047.46	250936.00	24.75	40.20	0.00	68.71	
	8	319735	308982	261156.21	319735.00	3.36	18.32	0.00	3499.81	
	9	386078	350520	295190.13	382840.50	9.21	23.54	0.84	113.66	
	10	408253	399790	334886.96	408253.00	2.07	17.97	0.00	594.47	
	11	460393	471774	396832.38	457155.50	-2.47	13.81	0.70	575.17	
	12	483876	406653	333722.33	478039.17	15.96	31.03	1.21	1623.56	

Parameter Transfer in CE-QAOA

We implemented *one-shot parameter transfer* as follows: for each instance size n we run CE-QAOA at $p = 1$ using a *fixed* angle pair (γ^*, β^*) imported from a generic $p = 1$ QAOA baseline, i.e., *without* any per-instance variational tuning (here `grid_evals` = 1). We then sample the resulting circuit, filter to feasible outcomes, and report the best feasible bitstring x_{best} by minimum energy. Empirically, this transfer already produces near-optimal solutions. CE-QAOA results in Table 7 shows exact optimal hits for $n \in \{3, 4, 5\}$ ($\text{gap}_{\text{best}} = 0$), and small approximation gaps for larger instances despite zero re-optimization. In particular, the best feasible energies satisfy $\text{gap}_{\text{best}} < 1\%$ for $n = 6, 7, 8, 9$ (0.04%, 0.25%, 0.21%, 0.73%, respectively) and remain close to optimal more broadly, with worst-case $\text{gap}_{\text{best}} \leq 1.64\%$ over $n \leq 12$. Conceptually, the transferred angles act as a coarse but effective “phase setting” for the CE kernel. The encoder and block-XY mixer confine dynamics to the one-hot manifold, the imported cost-phase still induces a useful phase gradient over low-penalty/low-cost regions, and the subsequent mixing concentrates weight on high-quality feasible assignments.